


Article

Vegetable Oil-Based Resins Reinforced with Spruce Bark Powder and with Its Hydrochar Lignocellulosic Biomass

Roxana Dinu ¹, Iuliana Bejenari ², Irina Volf ² and Alice Mija ^{1,*} 

¹ University Côte d'Azur, Institute of Chemistry of Nice, UMR CNRS 7272, CEDEX 02, 06108 Nice, France; Roxana.CONDRUZ@univ-cotedazur.fr

² Faculty of Chemical Engineering and Environmental Protection, Gheorghe Asachi Technical University of Iasi, 73 Prof. D. Mangeron Street, 700050 Iasi, Romania; iuliana.bejenari@tuiasi.ro (I.B.); ivolf@tuiasi.ro (I.V.)

* Correspondence: Alice.MIJA@univ-cotedazur.fr

Abstract: A bio-based polymeric matrix was developed by the copolymerization of a vegetable oil-based epoxy, epoxidized linseed oil (ELO), with dodecyl succinic anhydride (DDSA). To obtain eco-friendly bio-composites, this matrix was combined with a natural filler: spruce bark powder (SB) with its hydrochar (HC) in various proportions ranged from 1 to 30 wt.%. The reactivities of these formulations were studied by DSC analysis that highlighted that both fillers have a high catalytic effect on the ELO–DDSA crosslinking reaction. The complementary studies by TGA, DMA, tensile tests, water absorption and Shore tests had shown that both HC and SB bring improvements to the mechanical properties of the composites, fulfilling multiple roles: (i) Both act as co-reactants in the copolymerization mechanism; (ii) HC acts as reinforcement, consolidating the network and providing stiffness and rigidity; and (iii) SB acts as plasticizer for reducing the brittle character of the epoxy resins.



Citation: Dinu, R.; Bejenari, I.; Volf, I.; Mija, A. Vegetable Oil-Based Resins Reinforced with Spruce Bark Powder and with Its Hydrochar Lignocellulosic Biomass. *Appl. Sci.* **2021**, *11*, 10649. <https://doi.org/10.3390/app112210649>

Academic Editor: Ignazio Blanco

Received: 15 October 2021

Accepted: 10 November 2021

Published: 12 November 2021

Publisher's Note: MDPI stays neutral with regard to jurisdictional claims in published maps and institutional affiliations.



Copyright: © 2021 by the authors. Licensee MDPI, Basel, Switzerland. This article is an open access article distributed under the terms and conditions of the Creative Commons Attribution (CC BY) license (<https://creativecommons.org/licenses/by/4.0/>).

Keywords: vegetable oil; hydrothermal carbon; bio-composite; sustainable materials

1. Introduction

Polymeric materials have become increasingly attractive to a growing number of industrial sectors due to their unique properties, such as low weight, low or relatively low cost, easy processing and high flexibility to adapt the desired properties through a wide range of molecular changes [1]. Thermosetting polymers are highly crosslinked tridimensional structures that constitute about 20% of global plastic production, being widely used in engineering fields [2,3]. One of the most versatile classes of thermoset materials is represented by epoxy resins, which are widely used as adhesives for electronic components and circuits, semiconductor capsules, coatings, adhesives, structural materials in civil infrastructure, materials in the automotive and aerospace industries, composites, etc. [3–5]. This intensive use of epoxydic materials is due to their numerous qualities such as high chemical and mechanical strength, high thermal stability, high stiffness, good creep resistance, low shrinkage and good processability and compatibility with other polymers [2–6]. The majority of epoxy resins are based on bisphenol A (BPA) as their main compound, which has recently begun to be restricted due to its carcinogenic, mutagenic and reprotoxic (CMR) nature [7,8]. Therefore, to avoid the use of BPA and also to find alternatives to petrochemical resources creating problems of limited availability and volatile costs, academic and industrial studies on the development of new environmentally friendly epoxy materials from cheap, non-toxic, natural and renewable raw materials have intensified.

A renewable alternative for fossil derivatives is represented by vegetable oils. These are triglycerides which, due to their numerous reactive groups (double bonds, ester groups, etc.), can be easily chemically modified by numerous pathways (e.g., epoxidation) to develop new functionalities [9]. One of the main vegetable oils used in the development of thermosets is epoxidized linseed oil (ELO) [10]. Various academic studies have

been dedicated to develop thermoset resins based on ELO, with properties comparable to commercial ones [11–16]. Epoxidized linseed oil was also investigated as a potential matrix for the development of composites reinforced with fibres [17] or filled with micro- or nanoparticles [18,19].

The wood-based biomass is the major source of lignocellulosic fibres, intensely used for the production of pulp and paper, wood pellets and coal, but these industries also produce large amounts of residues such as, for example, the bark. Bark is the external layer of trees covering the stem, branches and roots, and it represents approximately 10% of the stem volume [20]. After peeling, a large amount of bark waste is produced, of which only a limited amount is used for bioenergy production or soil modification, while most of it is left to rot in the forest or burned to recuperate energy, losing an important source of lignocellulosic fibres [21]. Although there is a wide range of potential uses for this by-product, very few studies have been conducted on the valorisation of this industrial waste [22,23]. Another feasible valorisation method for this industrial by-product is by converting it, using different thermal methods, into interesting carbonaceous fillers that could replace the carbon nanotubes and graphene fibres [24–26]. These carbonaceous products, also called hydrochar or biochar, can be obtained through different thermochemical processes such as pyrolysis, gasification or hydrothermal carbonization [27,28]. The hydrothermal carbonization (HTC) process is considered to be the main process in the field of biomass use due to several advantages, such as being a cheap, environmentally friendly, non-toxic, green and easily applicable process [29]. Compared to other carbonization methods (incineration, pyrolysis and gasification), the HTC process can be operated at low temperatures ranged between 180 and 350 °C [30]. This process has also the advantage of allowing the use of wet biomass, as obtained from the technological scheme, without needing to apply a pre-drying step. The hydrochar obtained by this procedure is a carbon-rich product that has a wide range of uses, such as solid fuels, water treatment, soil amendment, bioenergy production and storage or biomedical field applications, but very few works refer to its use as reinforcing fibres in the development of epoxy polymeric composites [30–32].

The present work has as its principal objective the development of green and environmentally friendly composite materials that have in their composition a high percentage of bio-based, renewable and waste compounds as raw materials. Firstly, the bio-based epoxy matrix was developed starting from a commercially available vegetable oil, namely epoxidized linseed oil (ELO). Then, the designed epoxy-resin was loaded with different percentages (1–30 wt.%) of natural fillers: spruce bark powder (SB) or its hydrochar (HC) obtained by HTC treatment. The influence of the nature of the filler as well as of its ratios on the matrix's crosslinking were investigated by differential scanning calorimetry (DSC). After establishing the curing protocol, the SB- and HC-based materials were elaborated, and their physico-chemical and thermo-mechanical properties were carefully investigated by TGA, DMA, tensile tests, Shore tests and water absorption tests. The morphological characteristics and the compatibility and homogeneity between the filler and the matrix were analysed by scanning electron microscopy (SEM).

2. Materials and Methods

2.1. Materials

The epoxidized linseed oil (ELO) was supplied by Valtris Specialty Chemicals. This product appears as a yellow liquid with a viscosity of ~1200 Pa.s, a functionality of 5.5 epoxides per triglyceride and an average mass of 980 g·mol⁻¹. To develop the resin-based matrix, ELO was crosslinked with dodecanyl succinic anhydride (DDSA; 90%), with the reaction being initiated by an equal mixture of N,N'-dimethylbenzylamine (BDMA; initiator) and 2,4,6-tris(dimethylaminomethyl)phenol (DMP-30; accelerator). This ELO-based resin was used as the matrix for the composites' production, in which various proportions of hydrochar (HC) and spruce bark (SB) powder were used as green and sustainable fillers. Hydrochar (HC) was obtained from spruce bark powder by HTC process at 280 °C. HC appears as a brown powder with a particle size distribution of around 400 µm. The elemental

analysis of the synthesized HC and raw SB was investigated by energy-dispersive X-ray spectroscopy (EDX). The elemental content of HC is ~71.61% C, 21.11% O, 5.20% H, 1.44% Ca, 0.38% Cu and 0.26% Zn, while that of the SB is 58.26% C, 33.15% O, 5.84% H, 0.05% Mg, 0.01% Al, 0.01% Si, 0.04% P, 0.05% S, 0.01% Cl, 0.33% K, 1.59% Ca, 0.02% Mn, 0.38% Cu, 0.27% Zn.

2.2. Samples Elaboration

To prepare the polymeric matrix, a 1:1 stoichiometric ratio of the epoxy to the anhydride groups was used. The copolymerization reactions were initiated by 2.5 wt.% BDMA +2.5 wt.% DMP-30. For the composites' preparation, various proportions (1, 5, 10, 15, 20 and 30 wt.%) of SB and HC fillers were used. Firstly, the required amount of ELO was heated at 50 °C, and then the DDSA hardener was added and the mixture maintained on the heating plate under continuous stirring. The proper amount of filler was then added, the formulation being vigorously mixed. At the end, the mixtures were removed from the heating plate and the BDMA/DMP-30 mixture was added. The obtained mixtures were poured into silicon moulds and placed in an oven for curing and post-curing. In the curing step, the formulations were heated at 130 °C for 1 h 30 and for another hour at 160 °C. The post-curing reactions were done at 180 °C for 3 h. All the systems were coded based on their composition. The epoxy matrix was abbreviated with "EDI", the letter "E" being attributed to ELO, "D" to the anhydride and "I" for the equal mixture between BDMA and DMP-30. The natural fillers are denoted "HC" for hydrochar and "SB" for the spruce bark powder. The mass ratios of the component parts appear also in their name. For example, system "EDI80_HC20" is composed of 80 wt.% epoxy matrix (EDI) and 20 wt.% hydrochar (HC).

2.3. Experimental Section

2.3.1. Differential Scanning Calorimetry (DSC)

To establish the optimal crosslinking parameters and also to study the influence of filler on the thermal behaviour of the formulations, fresh samples (5–10 mg) were placed in 40 µL Al pans and tested using a DSC 3 Mettler Toledo instrument. All tests were performed under dynamic scan from 25 °C to 300 °C at 10 °C·min⁻¹ heating rate. Parameters such as reaction enthalpy (ΔH), maximum temperature of the reaction (T_{peak}) and interval of the reaction ($T_{\text{onset}} - T_{\text{end}}$) were recorded. The glass transitions ($T_{g\text{-DSC}}$) of the crosslinked samples were analysed by DSC applying two heating/cooling cycles from 25 °C to 200 °C at 10 °C·min⁻¹ rate, the values being considered as the inflection point of the DSC curves in the second heating scan.

2.3.2. Thermogravimetric Analysis (TGA)

Thermal stability of the bio-based resin and composites was studied in oxidative atmosphere from 25 °C to 1000 °C (10 °C·min⁻¹ heating rate) using a TGA 2 Mettler Toledo apparatus operated by STARe Software. The degradation temperature was recorded as the temperature at which materials lost 5% of their mass and was labelled with " $T_{5\%}$ ".

2.3.3. Dynamic Mechanical Analysis (DMA)

DMA technique was used to investigate relevant dynamic mechanical parameters such as storage moduli (E'), loss moduli (E'') and the damping factor ($\tan \delta = E''/E'$) of the designed resin and composites. The viscoelastic behaviour was studied under nitrogen atmosphere from -70 °C to 150 °C at a heating rate of 3 °C·min⁻¹ using a DMA 1 Mettler Toledo instrument. The samples were studied at an oscillatory frequency of 1.0 Hz and an amplitude of 20 µm. DMA data were used also for the calculation of the crosslink density of the systems and composites based on the following equation [33]:

$$v = \frac{E'}{3RT} \quad (1)$$

where E' is the storage modulus in the rubbery plateau at $T_g + 90$ °C (MPa), R is the universal gas constant, and T is the absolute temperature (K). Following the Tobolsky [34] relationship, the average molar mass between crosslinks of the epoxy-based resins was calculated using the equation:

$$Mc = \frac{3\rho RT}{E'} \quad (2)$$

$$Mc = \frac{\rho}{\vartheta} \quad (3)$$

where ρ is the calculated density ($\text{g}\cdot\text{cm}^{-3}$) and E' is the storage modulus in the rubbery plateau (MPa) at 130 °C.

2.3.4. Shore Hardness Tests

A ZwickRoell Hardness tester equipped with a Shore D device was used to investigate the fillers' influence on the hardness of the final materials. Flat samples were subjected to a load force of $50 \text{ N} \pm 0.5 \text{ N}$, and the hardness values were recorded at the firm contact between the device presser foot and the sample. To reduce human error, five measurements were recorded for each formulation and their average value calculated and given as the hardness of the materials.

2.3.5. Tensile Testing

Mechanical properties such as Young's modulus, tensile strength and elongation at break of the bio-resin and composites were explored by a mechanical universal testing machine Instron 34SC-5 operated by BlueHill software. Five samples for each formulation with the dimensions of $75 \times 10 \times 4 \text{ mm}$ [3] were tested, applying a crosshead speed of $10 \text{ mm}\cdot\text{min}^{-1}$, with the obtained values being averaged.

2.3.6. Water Absorption

Based on the ASTM D570 standard test method, rectangular samples of about $10 \times 8 \times 4 \text{ mm}^3$ were dried in oven at 50 °C for 24 h, then cooled and weighed, obtaining the initial mass " W_0 ". Then, the conditioned samples were immersed in deionized water at 23 ± 1 °C and maintained for 11 days. At each 24 h, samples were extracted from water, wiped carefully with filter paper, weighed (W_d), and again immersed in the container with water. The relative water absorption rate of the tested materials was determined using the equation:

$$\text{WA, \%} = \frac{W_d - W_0}{W_0} \times 100 \quad (4)$$

2.3.7. Scanning Electron Microscopy (SEM)

To study the samples' surface morphology and the fibre–matrix interaction, SEM analyses of the fractured surface were performed. Firstly, samples had been coated with platinum and thereafter analysed using a SEM Tescan Vega 3 XMU device at an acceleration voltage of 5 kV.

2.3.8. Energy-Dispersive X-ray Spectroscopy (EDX)

EDX analyses were performed with a Tescan Vega 3 XMU SEM equipped with an X-MaxN 50 EDX detector at accelerating voltages of 20 kV. EDX data were processed with the Aztec software (version 3.2, Oxford Instruments, Abingdon, UK).

3. Results and Discussions

3.1. Reactivity Studies by DSC Analyses

DSC analyses were performed on fresh mixtures to investigate the crosslinking reaction and the influence of the fillers' nature or ratio on reactions' enthalpy and temperature interval. In Figure 1 is represented the evolution of heat flow as a function of temperature

for the neat ELO-based thermosetting resin and for its formulations with SB and HC fillers. The obtained DSC data are tabulated in Table 1.

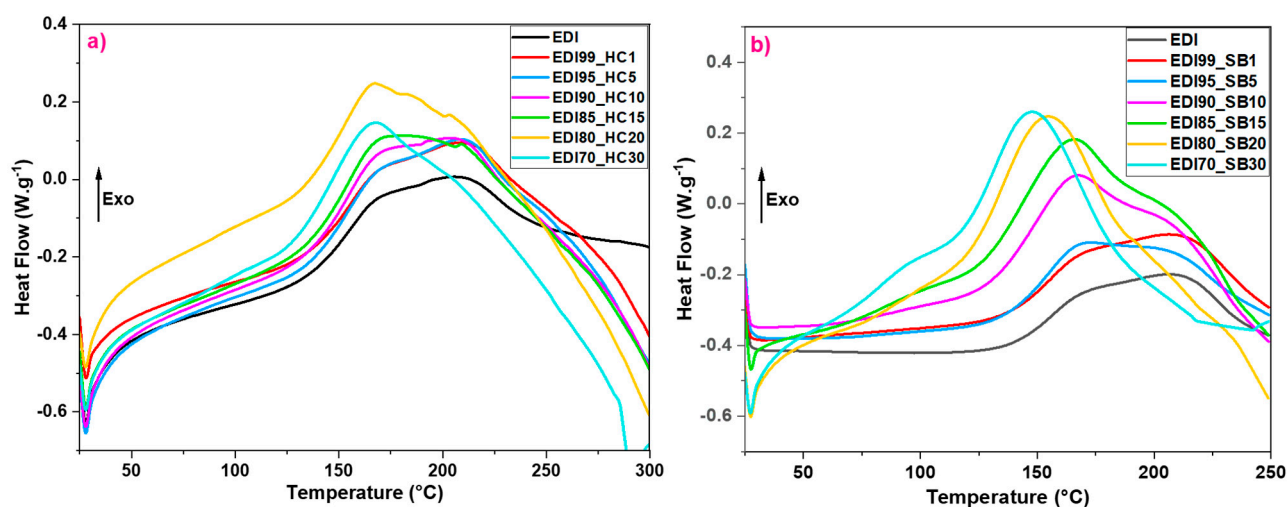


Figure 1. DSC thermograms during dynamic heating at $10\text{ }^{\circ}\text{C}\cdot\text{min}^{-1}$ of the epoxy-based formulation with (a) HC and (b) SB filler.

Table 1. DSC data obtained for the DSC curing of epoxy formulations with HC and SB.

Sample	$T_{\text{peak}}\text{ (}^{\circ}\text{C)}$ ($T_{\text{onset}}-T_{\text{end}}$) ($^{\circ}\text{C}$)	$\Delta H\text{ (J}\cdot\text{g}^{-1})$	Sample	$T_{\text{peak}}\text{ (}^{\circ}\text{C)}$ ($T_{\text{onset}}-T_{\text{end}}$) ($^{\circ}\text{C}$)	$\Delta H\text{ (J}\cdot\text{g}^{-1})$
EDI	194 (106–281)	92	EDI	194 (106–281)	92
EDI99_HC1	210 (86–291)	256	EDI99_SB1	206 (105–290)	102
EDI95_HC5	210 (73–293)	353	EDI95_SB5	172 (105–285)	110
EDI90_HC10	205 (67–292)	377	EDI90_SB10	168 (75–275)	251
EDI85_HC15	186 (63–290)	407	EDI85_SB15	166 (61–250)	337
EDI80_HC20	184 (58–290)	546	EDI80_SB20	155 (59–237)	356
EDI70_HC30	168 (52–284)	608	EDI70_SB30	148 (50–218)	364

The epoxy–anhydride crosslinking process is displayed as a broad exothermic peak, with its first peak at around $165\text{ }^{\circ}\text{C}$. These thermograms reveal the presence of complex epoxy–anhydride reactions initiated by a tertiary amine [35,36]. The copolymerization reaction of ELO–DDSA starts at around $106\text{ }^{\circ}\text{C}$, reaching the maximum reactivity at $194\text{ }^{\circ}\text{C}$ and finishing at around $280\text{ }^{\circ}\text{C}$. Based on the DSC thermograms from Figure 1a,b, it can be seen that the addition of both SB and HC fillers greatly influences the shape of curing reaction curves.

The reaction enthalpy of the systems was determined by integrating the area under the exothermic peak and normalizing it to the mass of resin. According to the literature studies [37,38], the T_{peak} temperature obtained by DSC analyses is considered a criterion for evaluating the reactivity of the systems; the lower the value of T_{peak} , the higher the reactivity. Figure 2 displays the evolution of the reaction enthalpy (ΔH) and maximum temperature of the reaction (T_{peak}) of the systems as a function of the filler's nature and ratio.

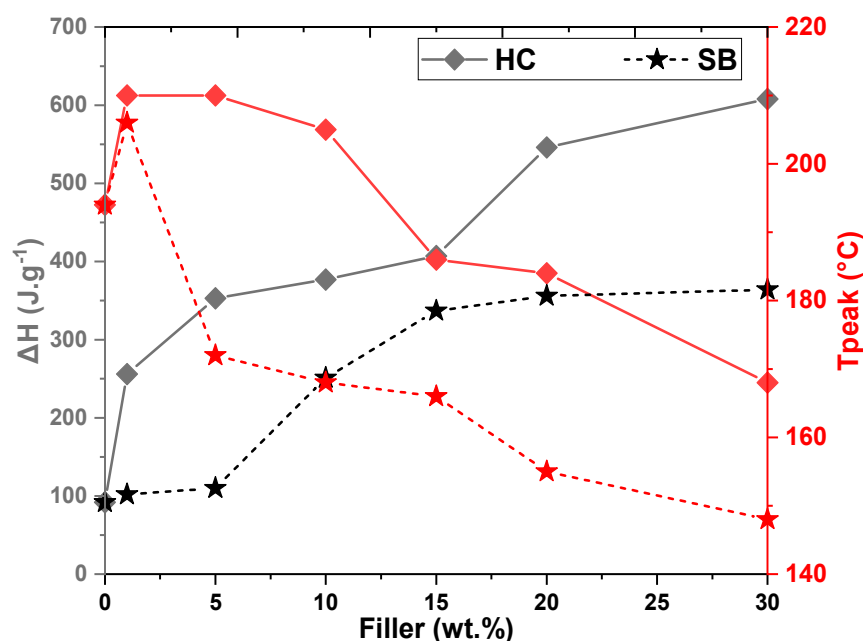


Figure 2. Evolution of the enthalpy of reaction (ΔH ; black line) and the maximum temperature of reaction (T_{peak} ; red line) as a function of filler ratio.

From Figure 1 and Table 1, we can observe firstly that the formulations with the two fillers, SB and HC, react following the EDI system behavior, i.e., with a complex multippeak evolution of the heat flow. In contrast, we can observe that the fillers' presence modifies the reactions' temperature intervals, enthalpy and the amplitude of the first peak at around 160 °C. With the increase of the amount of HC and SB, the curing reactions start at lower temperatures. For example, if the crosslinking reaction of EDI formulation begins at about 106 °C, the addition of 30 wt.% natural filler decreases the reaction onset to 52 °C for the EDI70_HC30 system and 50 °C for EDI70_SB30. The temperature at which the systems reach a quasi-linear response and the ends of their reactions is not influenced by the HC addition, but with the increase of the spruce bark amount, the T_{end} temperature is significantly reduced to 218 °C for the formulation with 30 wt.% SB.

As can be seen in Figure 2, the maximum temperature of the reaction for the systems with low amounts of HC (1, 5 and 10 wt.%) is shifted to higher temperatures (205–210 °C), but with the increase of HC quantity at 15, 20 and 30 wt.%, a constant decreasing of T_{peak} and increasing of reactivity can be observed. For the formulations with spruce bark powder, the maximum temperature of the reaction increased only for the mixture with 1 wt.% filler ($T_{peak} = 206$ °C), while for the other systems (from 5 to 30 wt.%), T_{peak} was shifted to lower temperatures, reaching up to 148 °C for the formulation with 30 wt.% SB.

Based on the DSC data listed in Table 1, the reaction enthalpy of ELO-based resin is about 92 J·g⁻¹, while the addition of only 1wt.% HC doubled the reactivity of the system, reaching values of about 608 J·g⁻¹ for the formulation with 30% by weight HC. The addition of spruce bark powder also led to an increase in reactivity, but it was lower compared to that of HC systems, with the enthalpy of reaction reaching 300 J·g⁻¹ for the mixture with 30 wt.% SB. This high increase in curing reaction enthalpy of ELO/DDSA in the presence of HC and SB, corroborated with the decreased onset of temperature reactions, shows a catalytic effect of both fillers, and moreover, perhaps a sign of their chemical bonding may be due to the presence of several reactant particles that have the energy to combine and increase reaction rates, such as the formation of new chemical bonds by the interaction of residual –OH groups with the epoxy groups. The higher reaction enthalpy of HC-filled systems compared to those containing SB can be explained probably by a combined chemical and physical effect [39,40]. As we can observe from elemental analysis, the HTC process was mild, with the elemental content of HC still being rich in oxygen

(21.11%), and hydrogen (5.20%), a sign of the presence of oxygenated functional groups. The reactivity of these functional groups present on HC is probably also higher than those on SB due to the HC's enlarged specific surface. This result is highlighted in Figure 2, where we can clearly observe that the increase of the fillers' content produces a high increase in reactions' enthalpy at the same time as the decreases of peak temperature and reaction onset, as previously discussed.

Consequently, based on DSC analyses, it was found that both HC and SB substantially influence the crosslinking parameters of the systems, confirming the chemical contribution of the filler as a catalyst in the copolymerization process.

3.2. Thermogravimetric Analysis Results (TGA)

Graphical representations of the mass loss as a function of temperature for the designed polymeric materials are illustrated in Figure 3. The thermal decompositions of the raw SB and HC fillers were also investigated, with the corresponding TGA/DTG curves being plotted in Figure 4.

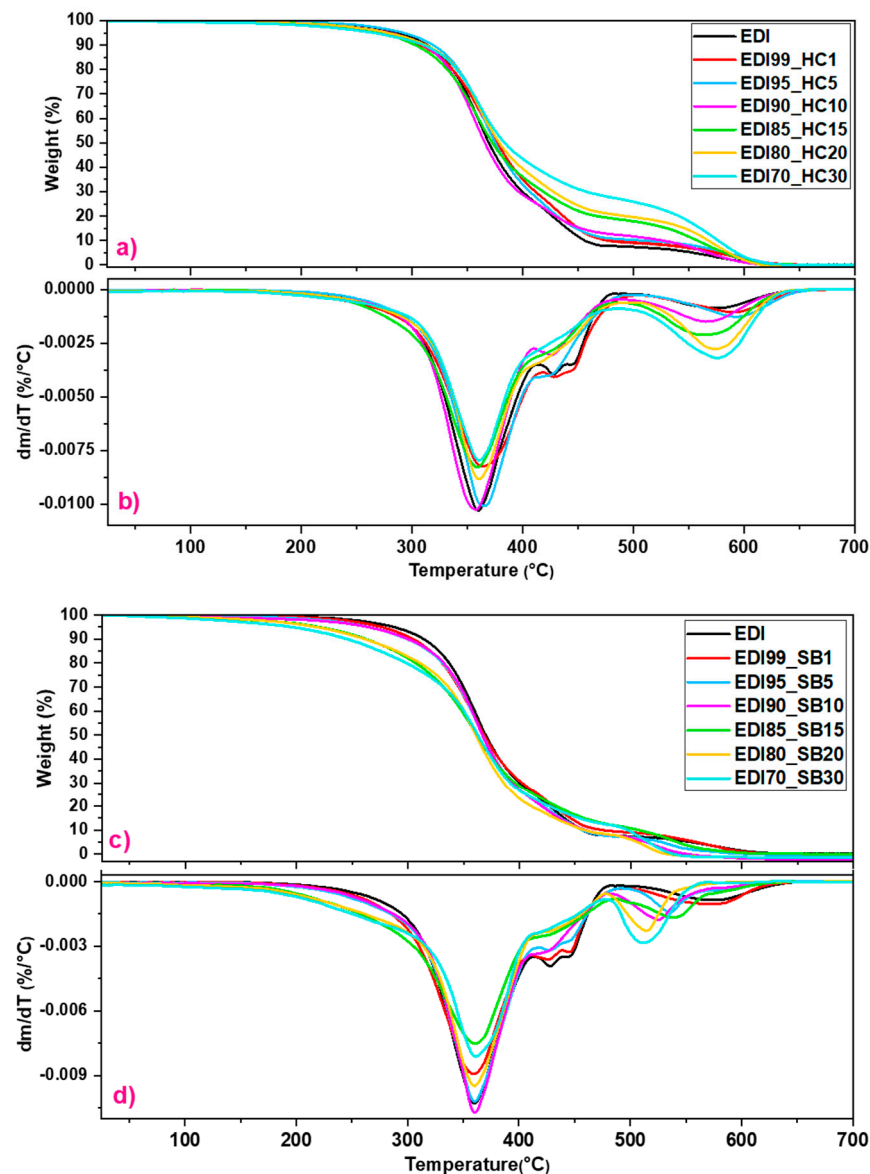


Figure 3. TGA/DTG curves for the (a,b) HC-based materials and (c,d) SB-based materials in oxidative environment, heating at 10 °C/min.

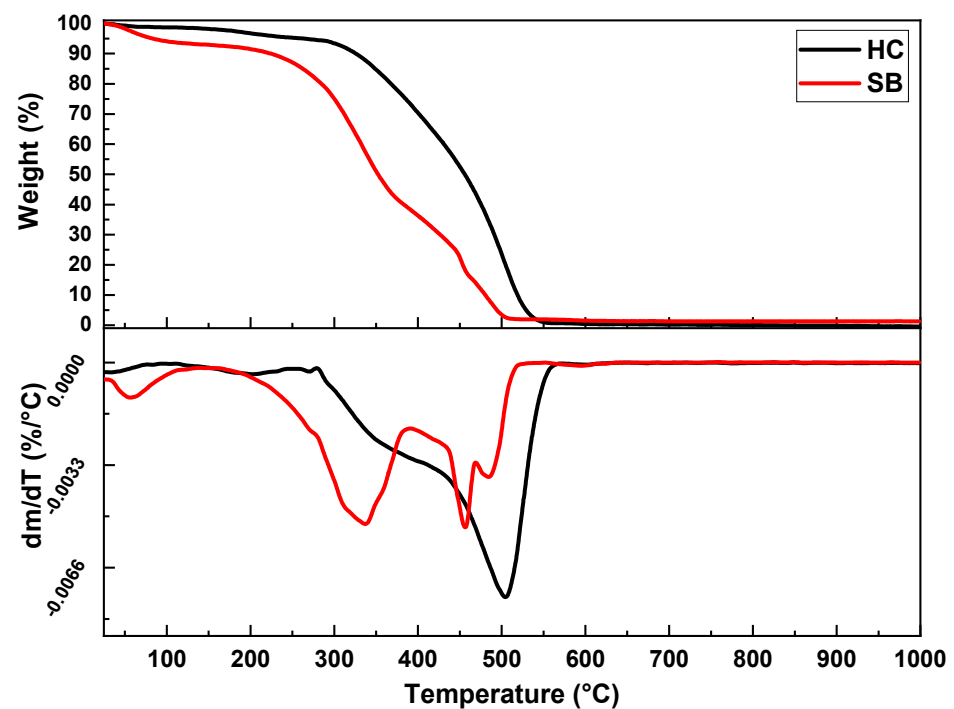


Figure 4. TGA and DTG curves for raw HC (black line) and raw SB (red line).

Generally, wood biomass is constituted mainly by hemicellulose, cellulose, lignin and small percentages of other organic and inorganic extractives [41]. Based on the literature study [42,43], softwood is composed of 18–38% cellulose, 15–33% hemicellulose and about 30–60% lignin. The TGA/DTG thermograms (Figure 4) of raw SB and HC present several mass losses. The first mass loss observed for both raw SB and HC is presented from 35–40 °C to 120–140 °C and is attributed to the evaporation of the absorbed water. Thermal treatment applied to obtain the HC particles influenced the mass loss at this stage, which is only 1%, compared to the raw SB, which loses about 7%. TGA analyses (Figure 4) show that the thermal stability of SB is divided into two distinct and complex stages, while in the case of HC, this behaviour appears as a broad and complex degradation mechanism step. According to the literature [44–46], the thermal behaviour of the lignocellulosic biomass is characterized by a two-step process, the first one (200–370 °C) being attributed to the depolymerization of hemicellulose and the breaking of glycosidic bonding of cellulose, while the main thermal degradation stage (340–370 °C) is characteristic of the degradation of α -cellulose. Due to its complex structure, the thermal degradation of lignin takes place at a large range of temperatures (200–500 °C) interposing with that of cellulose and hemicellulose. For the raw SB, the second degradation stage is ranged between 170 and 390 °C, with a mass loss of about 56%, while the cellulose and lignin degradation for this natural filler appears as a double broad peak from 400 °C to 540 °C, having a mass loss around 37%. Knowing that hemicelluloses are less thermally stable than cellulose and lignin, starting their decomposition at about 160 °C [47], the thermal treatment at 280 °C applied for HC manufacturing led to the degradation and partial removal of the hemicellulose. Therefore, the thermal decomposition of raw HC appears as a single broad peak, ranged from 250 °C to 580 °C, with a mass loss of ~95%.

Studying the DTG curves (Figure 3b,d), it can be seen that the thermal decompositions of the ELO-based resins and composites are divided into two major stages. Before the main degradation step, a small mass loss of about 3–6% appears for all the systems in the temperature interval of 140–260 °C, typical for the gradual evaporation of absorbed water and the release of volatiles present in the materials' compositions. The first major degradation step shows up as a complex exothermic peak with a double peak shoulder. This principal thermal step is ranged in the 260–500 °C temperature interval, with a maximum

temperature of degradation at about 365 °C and a mass loss of ~75–90%, and is characteristic of the thermolysis of network structure [48]. The thermo-oxidative degradations take place in the last stage of decomposition, ranged from 500 to 700 °C with a maximum at ~540–590 °C, presenting a mass loss of about 7–22%. As can be seen, the thermal stability of the developed materials is improved with the addition of filler; as the amount of HC or SB increases, the mass loss in the first stage decreases and increases in the second, which occurs at higher temperatures.

The thermal degradation was established by convention to be located at the temperature at which the sample lost 5% of its mass and was noted with “ $T_{5\%}$ ”, with the obtained values being tabulated in Table 2. EDI resin has a very good thermal stability, losing 5% of its mass at temperatures above 280 °C. Analysing the systems with HC, it is observed that the addition of filler slightly reduced the thermal stability of the materials, with $T_{5\%}$ being between 262–280 °C. In fact, in the case of the material filled with 5 wt.% HC, the thermal stability was improved, being higher by about 10 °C than that of the neat epoxy resin ($T_{5\%} = 282$ °C). Instead, the SB filler led to a gradual decrease in thermal stability of the composites’ materials, reaching up to $T_{5\%} = 192$ °C in the case of formulation with 30 wt.% spruce bark particles, showing the contribution of the lignocellulosic component.

Table 2. Physico-chemical and thermo-mechanical properties of the samples.

Sample	Density (g/cm ³)	T_{g-DSC} (°C)	$T_{5\%}$ (°C)	Tan δ (°C)	Tan δ Peak Height	E' at 25 °C (MPa)	E' at 150 °C (MPa)	ν (mmol·cm ⁻³)	Mc (g/mol)	Hardness Test (Shore D)
EDI	0.9456	45	282	42	0.63	242	11	0.93	930	63
EDI99_HC1	1.2627	43	274	24	0.61	58	11	1.14	1255	65
EDI95_HC5	1.1317	31	291	29	0.58	98	13	1.11	946	75
EDI90_HC10	1.1401	38	280	36	0.58	260	17	1.03	697	80
EDI85_HC15	1.1745	35	271	43	0.54	560	26	0.88	694	81
EDI80_HC20	1.1174	37	273	45	0.53	727	40	0.23	290	85
EDI70_HC30	1.0528	33	262	43	0.47	911	68	0.22	161	84
EDI99_SB1	1.2901	31	274	49	0.77	700	11	1.15	1123	64
EDI95_SB5	1.0331	31	263	47	0.89	790	11	1.10	938	75
EDI90_SB10	1.1288	30	261	42	0.91	850	10	1.02	1100	77
EDI85_SB15	1.1571	27	221	40	1.15	550	9	0.87	1330	84
EDI80_SB20	1.0284	25	218	37	1.22	330	2	0.24	4432	80
EDI70_SB30	1.0192	20	192	40	1.22	545	2	0.23	4464	84

3.3. Dynamical Mechanical Analysis (DMA)

The materials’ properties, such as the storage modulus (E'), loss modulus (E'') and the damping factor (tan δ) of the ELO-based resin and composites, were studied by DMA (Figure 5). From the thermomechanical data given in Table 2, we can see that both the nature and the quantity of the filler influence the materials’ behaviour.

Considering the glassy region of the storage modulus, the addition of 1 and 5 wt.% HC led to a substantial decrease of the E' value, but starting with the material with 10 wt.% HC in its composition, the E' modulus increases considerably with the hydrochar amount. Therefore, when HC is in small quantities in the formulation composition, it fully participates in the copolymerization process, generating new polymeric structures. As the amount of hydrochar increases, the system becomes supersaturated, and the particles that have not chemically interacted act as filler, giving rigidity to the material. In the case of SB-based systems, the storage modulus in the glassy state increases significantly compared to the resin, but its value is influenced by the filler amount. For the materials with 1–10 wt.% SB, the E' value is doubled and even tripled compared with the resin, and then it decreases suddenly starting with the materials filled with 15 wt.% spruce bark powder. This decrease may be due to the agglomeration of wood particles in the polymeric matrix, which may

lead to a steric hindrance, blocking some sites from forming new chemical bonds. This result corroborates the calculated crosslink densities (Table 2) that increase from 1 to 10% of filler ratio, and thereafter, in both cases the values decrease. The storage modulus at room temperature for the ELO-based matrix is about 242 MPa, while in the case of the HTC-based system, the highest E' value is reached by the formulation with 30 wt.% HC (~911 MPa), and for the SB-based systems, the maximum is reached by the formulation filled with 10 wt.% SB (~850 MPa).

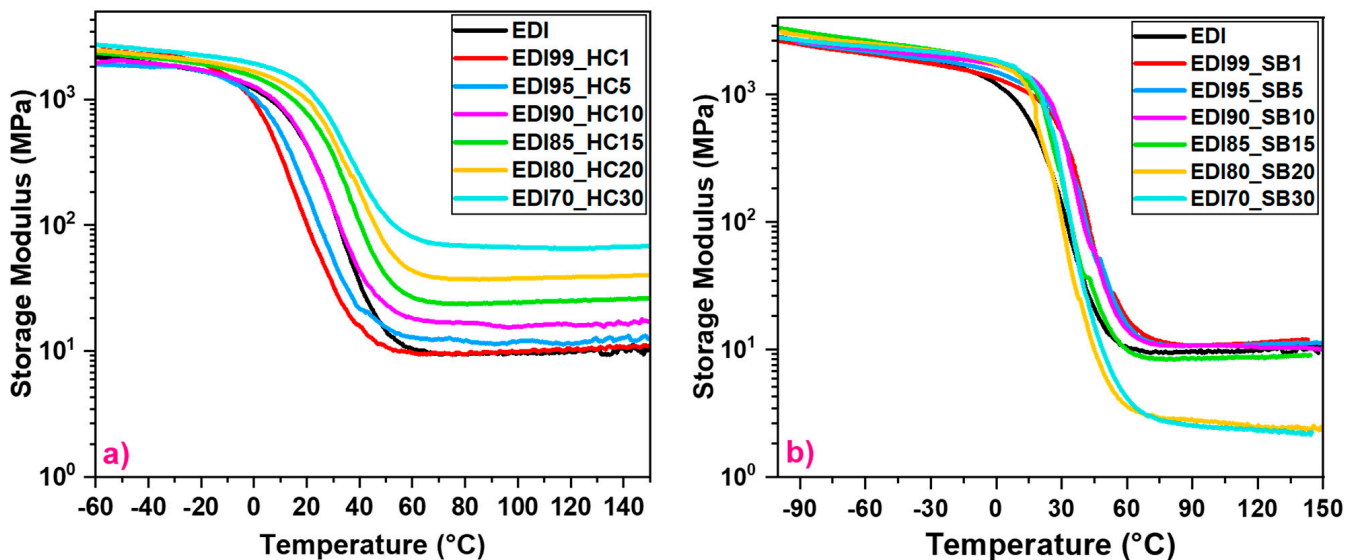


Figure 5. Storage modulus (E') vs. temperature curves of the (a) HC-based samples and (b) SB-based samples.

The storage modulus in the rubbery plateau of the designed polymeric systems was also analysed. For HC-based materials, the addition of filler increased E' in the rubber region, improving the stiffness of the formulations, so HC has a reinforcement effect. Instead, the addition of SB in the ELO-based matrix decreases the value of E' in this region, with the SB particles giving a plasticizing effect to the composite material.

The damping factor ($\tan \delta$) so-called also α relaxation (cooperative motions of main chain) of the systems with HC and SB were investigated and are represented in Figure 6. The maximum values of the $\tan \delta$ peaks, which are associated with the macroscopic glass transition (T_g), were recorded from DMA analysis, and the obtained data are collected in Table 2. The $\tan \delta$ of the EDI resin is ~42 °C, while the addition of 1 wt.% HC decreased the $\tan \delta$ to ~24 °C. By increasing the HC%, the $\tan \delta$ values increase, and this became superior to that of neat resin at >15 wt.% HC ($\tan \delta = 43$ °C), presenting the maximum value for the system with 20 wt.% HC ($\tan \delta = 45$ °C). In contrast, the addition of SB has an opposite effect on the $\tan \delta$ values: the maximum value of the damping factor is reached for the composite with 1 wt.% SB; thereafter, $\tan \delta$ values gradually decrease with SB% increasing, with the lowest value being ~37 °C for the formulation with 20 wt.% SB.

The hardness of the samples was studied by using the Shore hardness tests with a Shore D device. The hardness value of the EDI resin is ~63 SD, a value indicating a medium hard material. The addition of HC and SB produces an increase in the composites' hardness, with the composites showing values ranging between 65 and 85 SD for HC-based materials and between 64 and 84 SD for SB-based materials.

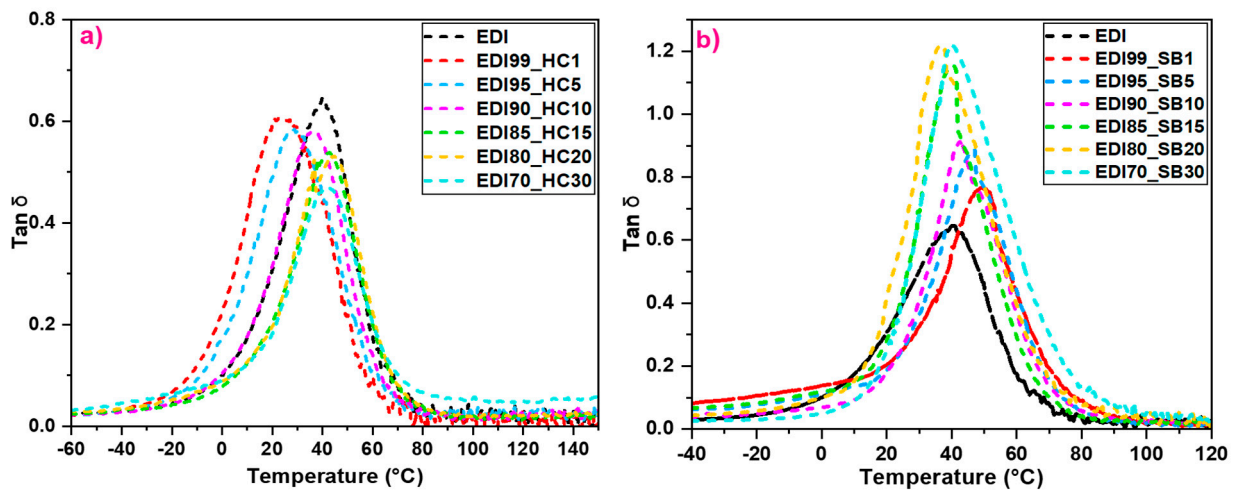


Figure 6. Damping factor as a function of temperature for (a) HC-based materials and (b) SB-based materials.

3.4. Tensile Tests

For a better characterization and for easier framing of an applicability area, the mechanical properties of the materials were analysed by tensile tests. The stiffness of the materials, known as Young's modulus, the tensile strength and the elongation at break for all the systems were investigated, with the experimental data being shown in Figure 7 and Table 3.

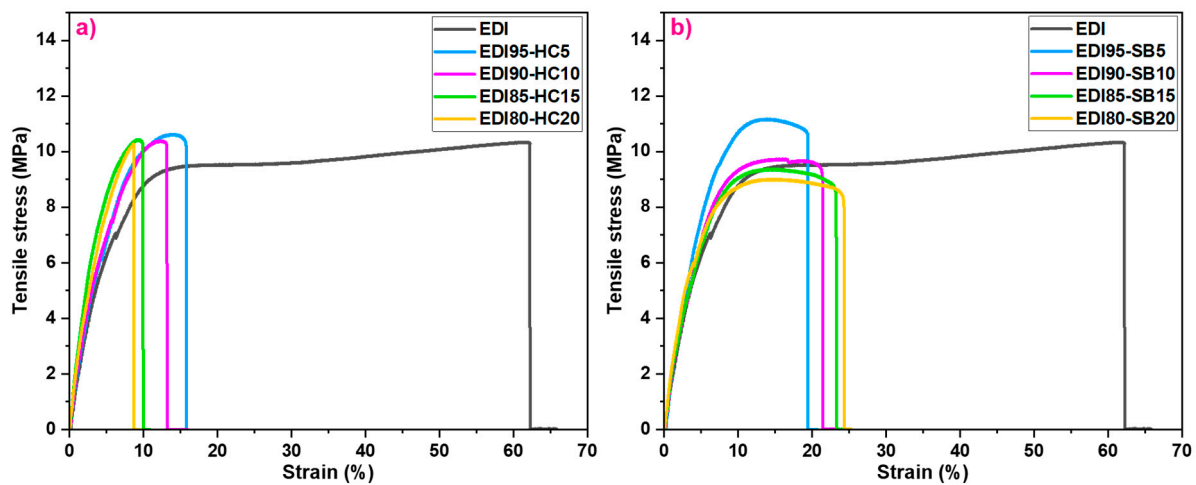


Figure 7. Stress–strain curves of the (a) ELO/HC-based composites and (b) ELO/SB-based composites.

Table 3. Tensile test data and brittleness values of the samples.

	Young's Modulus (MPa)	Tensile Stress (MPa)	Tensile Strain (%)	B (%·Pa/10 ¹⁰)
EDI	178.06 ± 40.69	10.33 ± 2.32	61.87 ± 6.65	0.06
EDI95_HC5	202.83 ± 28.55	13.91 ± 1.89	15.84 ± 2.33	0.64
EDI90_HC10	225.30 ± 22.77	12.13 ± 2.54	13.82 ± 1.82	0.28
EDI85_HC15	292.40 ± 87.17	9.20 ± 3.15	10.11 ± 5.93	0.18
EDI80_HC20	266.50 ± 13.86	8.66 ± 2.85	10.89 ± 0.44	0.16
EDI95_SB5	232.12 ± 33.09	11.14 ± 1.95	19.70 ± 1.37	0.07
EDI90_SB10	223.88 ± 7.98	9.70 ± 2.62	20.74 ± 4.04	0.06
EDI85_SB15	231.35 ± 13.51	9.45 ± 3.06	21.20 ± 6.94	0.09
EDI80_SB20	237.94 ± 9.41	8.99 ± 2.76	22.98 ± 6.59	0.13

The mechanical properties of the composites' materials are influenced by various factors, such as the manufacturing and processing parameters, the filler nature and content, the polymeric matrix, the compatibility between the matrix and filler, etc. [49]. From Figure 7, we can observe that the EDI resin has good mechanical properties, showing a tensile stress value of about 10 MPa and a very high elongation at break of about 62%. With the addition of the filler, an increase in the tensile stress values can be observed only up to a certain load, such as for materials with 5 and 10 wt.% HC (~12–14 MPa) and for the ones filled with 5 wt.% SB (~11MPa). For the systems filled with 15–20 wt.% HC and 10–20 wt.% SB, the tensile stress properties slightly decreased, varying between 8.6 and 9.2 MPa for HC-based samples and between 8.9 and 9.7 MPa for SB-based samples. The elongation at break of the materials also decreased considerably with the increase of the filler amounts (10–16% for HC systems; 20–23% for SB systems), thus giving rigidity to the samples.

The stiffness of the developed materials, also called Young's modulus, is defined by the relationship between stress and deformation in the regime of linear elasticity of a uniaxial deformation, and the obtained values are tabulated in Table 3. Based on the obtained data, it can be seen that the natural filler addition improved the Young's modulus values. For example, the stiffness value for the EDI resin is about 180 MPa, while the addition of 15 wt.% HC led to an increase to the Young's modulus value to about 300 MPa. The addition of spruce bark powder also led to the improvement of the mechanical properties, with 20 wt.% SB improving the stiffness of the final materials to about 270 MPa.

Based on the data obtained from tensile test and DMA analyses, the brittleness (B) of the designed materials was also calculated using the equation:

$$B = 1/\varepsilon_b E' \quad (5)$$

where ε_b is the elongation at break obtained by tensile testing and E' represents the storage modulus value at 25 °C obtained by DMA. According to the literature studies [50–52], it is known that the brittleness parameter is inversely proportional to the E' modulus at a frequency of 1.0 Hz, and the lower the value of the brittleness of the analysed materials, the greater their dimensional stability.

Therefore, the addition of an optimal amount of HC or SB as fillers in the ELO-based matrix leads to the improvement of the mechanical properties of the final materials, increasing the Young's modulus and tensile stress.

3.5. Water Absorption

The sorption characteristics were investigated by a gravimetric analysis according to the standards provided by ASTM D570. The percentage of water absorbed by the designed materials after 11 days of immersion at room temperature is represented graphically in Figure 8. Based on the literature studies [53–58], it is known that the moisture absorption of polymeric materials is influenced by numerous factors, the principal ones being the presence of nanovoids and microcracks characteristic for epoxy resins and the presence of hydroxyl or other polar groups in the chemical network. As can be seen in Figure 8, the water retention of the neat EDI resin is very low, with the WA% being about 0.7% at saturation level. If we analyse the water absorption depending on the nature of the filler, as both HC and SB present hydroxyl groups along the chain, they will increase the affinity of composites for water. Thereafter, in the case of untreated wood filler SB, the concentration of polar groups is higher than that of HC, leading to higher water absorption.

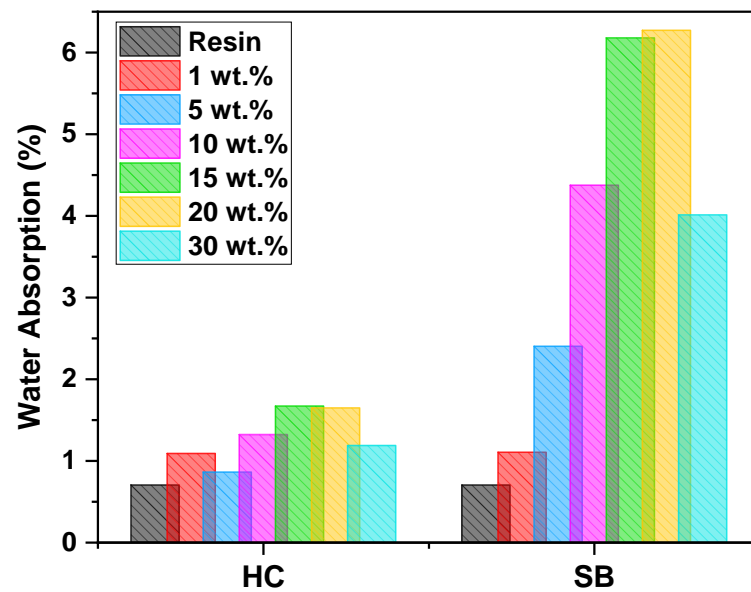


Figure 8. Water absorption of the ELO/HC and ELO/SB polymeric materials after 11 days of immersion in deionized water at room temperature.

Investigating the water retention behaviour depending on the amount of filler, the WA% gradually increases with the increase of the filler quantity. In addition to the presence of polar groups that favour water absorption by hydrogen bonding, the manufacturing protocol of the polymeric materials, as well as the presence of some chemically unbound filler particles, can lead to the formation of microcracks that favour the penetration of water through the network. In the case of both HC and SB composites, the maximum WA% at saturation level is reached by the systems with 20 wt.% filler, being around 1.7% for HC materials and 6.3% for SB materials. For the materials with 30 wt.% filler, a decrease of the WA% can be observed, which may be due to the supra-saturation of the network.

In conclusion, the designed materials reveal a very good WA% at the saturation level, ranged between 0.7 and 1.7% for the ELO/ HC composites and between 0.7% and 6.3% for those with SB.

3.6. SEM

The surface morphology of the fractured samples was analysed by SEM, as presented in Figure 9 for ELO/HC composites, while ELO/SB composites are displayed in Figure 10. It can be seen that both HC and SB composites present a good inclusion of natural particles in the polymeric matrix. The original fibre skeleton and honeycomb structure of the spruce wood can be also observed (Figure 10d) [56].

The presence of the epoxy resin inside of the wood cells (Figure 10d,e) confirms a very good compatibility and impregnation of the wood particles with the resin, which confers a strong interfacial bonding between polymers reinforced by SB. As we can observe in Figures 9 and 10, the surfaces of the HC and SB fibres are very well covered with resin, and the total lack of voids at the resin–fibre interface denotes a very good compatibility between the epoxy matrix and the HC and SB particles. Additionally, the EDI resin reveals a smooth and homogeneous surface. The presence of microcracks on the materials' surface may be due to the manufacturing process or the method of sampling of the analysed samples.

Therefore, the HC and SB fillers present an excellent compatibility with the ELO-based matrix, leaving the resin to penetrate inside the pores, creating physical and mechanical bonding. The uniform and homogeneous distribution of the filler in the polymeric matrix, as well as the good adhesion between the two compounds, led to the generation of green composites.

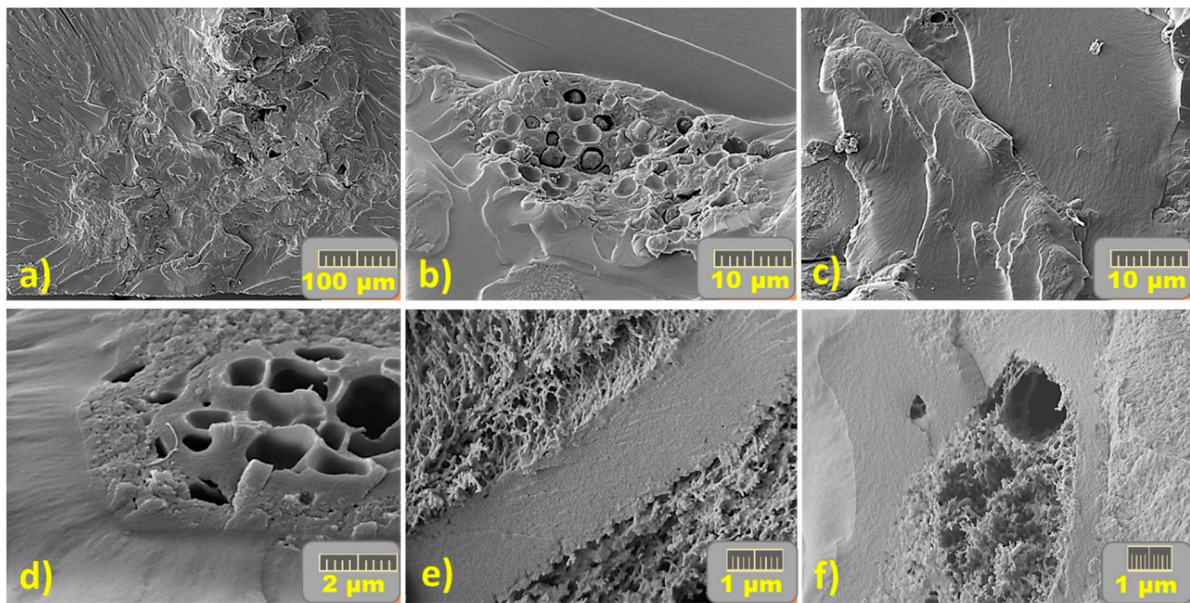


Figure 9. SEM micrograph of the ELO-based formulations filled with HC at (a) 100 μm , (b) and (c) 10 μm , (d) 2 μm , (e, f) 1 μm .

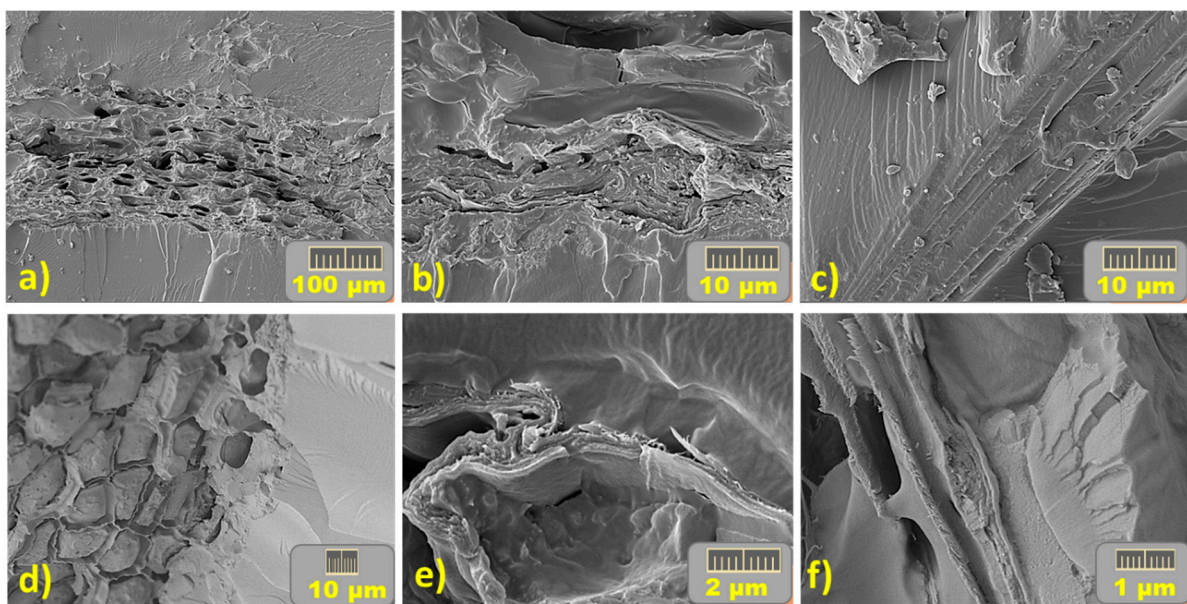


Figure 10. SEM micrograph of the ELO-based formulations filled with SB at (a) 100 μm , (b–d) 10 μm , (e) 2 μm , and (f) 1 μm .

4. Conclusions

Bio-based eco-friendly composites were designed and elaborated by combining a vegetable oil-based epoxide, ELO, with spruce bark wood, SB, and its hydrochar, HC, in the presence of DDSA anhydride as a hardener. The reactivity of formulations containing from 0 to 30% HC and SB fillers was studied with the help of DSC, with the results showing a high catalytic effect of both fillers on the ELO crosslinking reaction. Indeed, the enthalpy of reaction is 6.6 times higher for the formulation with 30% HC compared with that of the neat resin (i.e., 608 vs. 92 $\text{J}\cdot\text{g}^{-1}$) and almost four times higher in the case of formulation with 30% SB (364 vs. 92 $\text{J}\cdot\text{g}^{-1}$). The onset of the reactions' temperatures had also been influenced, being decreased for the both HC and SB systems. These results are a clear sign that both HC and SB contribute to the chemical mechanism of ELO crosslinking. Not only were the chemical reactivities influenced by the two fillers, but also the final properties of

the produced composites. The storage modulus in the rubbery plateau increases with HC% in composites, a sign of a reinforcement of the material's stiffness.

Based on the Shore hardness test, the inclusion of both SB and HC in the epoxy-based matrix improved the hardness of the materials from 63 SD (neat resin) to 84–85 SD for the composites with 30 wt.% filler. By tensile test, an improvement of the mechanical properties was also observed, with the Young's modulus increasing from 180 MPa (neat resin) to 300 MPa for the sample with 15 wt.% HC and 270 MPa for the one with 20 wt.% SB. The influence of the natural fillers on the water absorption behaviour at the saturation level (after 11 days of immersion) was also investigated, revealing a low water retention with values ranged between 0.7 and 1.7% for HC materials and between 0.7 and 6.3% for SB composites. Depending on this parameter, the materials with HC and low SB quantity can be easily used in outdoor applications, while materials with higher concentrations of SB that have a slightly higher WA% can be intended for indoor use. SEM analysis revealed a very good interaction between the matrix and fibres and also a good distribution and homogeneity of the particles in the system.

Author Contributions: R.D.: formal analysis; investigation; data curation; writing—original draft preparation; methodology; I.B.: formal analysis; investigation; data curation; I.V.: validation; supervision; A.M.: Conceptualization; methodology; validation; supervision; resources; writing—review and editing; project administration. All authors have read and agreed to the published version of the manuscript.

Funding: This research received no external funding.

Institutional Review Board Statement: Not applicable.

Informed Consent Statement: Not applicable.

Data Availability Statement: Not applicable.

Conflicts of Interest: The authors declare no conflict of interest.

References

1. Ratna, D. *Handbook of Thermoset Resins*; Smithers Rapra: Shrewsbury, UK, 2009.
2. Ng, F.; Couture, G.; Philippe, C.; Boutevin, B.; Caillol, S. Bio-Based Aromatic Epoxy Monomers for Thermoset Materials. *Molecules* **2017**, *22*, 149. [[CrossRef](#)]
3. Ramon, E.; Sguazzo, C.; Moreira, P. A Review of Recent Research on Bio-Based Epoxy Systems for Engineering Applications and Potentialities in the Aviation Sector. *Aerospace* **2018**, *5*, 110. [[CrossRef](#)]
4. Wan, J.; Zhao, J.; Zhang, X.; Fan, H.; Zhang, J.; Hu, D.; Jin, P.; Wang, D.Y. Epoxy Thermosets and Materials Derived from Bio-Based Monomeric Phenols: Transformations and Performances. *Prog. Polym. Sci.* **2020**, *108*, 101287. [[CrossRef](#)]
5. Paolillo, S.; Bose, R.K.; Santana, M.H.; Grande, A.M. Intrinsic Self-Healing Epoxies in Polymer Matrix Composites (Pmcs) for Aerospace Applications. *Polymers* **2021**, *13*, 201. [[CrossRef](#)] [[PubMed](#)]
6. Mashouf Roudsari, G.; Mohanty, A.K.; Misra, M. Green Approaches To Engineer Tough Biobased Epoxies: A Review. *ACS Sustain. Chem. Eng.* **2017**, *5*, 9528–9541. [[CrossRef](#)]
7. Moreman, J.; Lee, O.; Trznadel, M.; David, A.; Kudoh, T.; Tyler, C.R. Acute Toxicity, Teratogenic, and Estrogenic Effects of Bisphenol A and Its Alternative Replacements Bisphenol S, Bisphenol F, and Bisphenol AF in Zebrafish Embryo-Larvae. *Environ. Sci. Technol.* **2017**, *51*, 12796–12805. [[CrossRef](#)]
8. Vandenberg, L.N.; Hauser, R.; Marcus, M.; Olea, N.; Welshons, W.V. Human Exposure to Bisphenol A (BPA). *Reprod. Toxicol.* **2007**, *24*, 139–177. [[CrossRef](#)]
9. Auvergne, R.; Caillol, S.; David, G.; Boutevin, B.; Pascault, J.P. Biobased Thermosetting Epoxy: Present and Future. *Chem. Rev.* **2014**, *114*, 1082–1115. [[CrossRef](#)]
10. Narine, S.S.; Kong, X. Vegetable Oils in Production of Polymers and Plastics. In *Bailey's Industrial Oil and Fat Products*; Shahidi, F., Ed.; John Wiley & Sons, Inc.: Hoboken, NJ, USA, 2005; pp. 279–306. [[CrossRef](#)]
11. Di Mauro, C.; Genua, A.; Mija, A. Building Thermally and Chemically Reversible Covalent Bonds in Vegetable Oil Based Epoxy Thermosets. Influence of Epoxy–Hardener Ratio in Promoting Recyclability. *Mater. Adv.* **2020**, *1*, 1788–1798. [[CrossRef](#)]
12. Todorovic, A.; Resch-Fauster, K.; Mahendran, A.R.; Oreski, G.; Kern, W. Curing of Epoxidized Linseed Oil: Investigation of the Curing Reaction with Different Hardener Types. *J. Appl. Polym. Sci.* **2021**, *138*, 50239. [[CrossRef](#)]
13. Pin, J.M.; Sbirrazzuoli, N.; Mija, A. From Epoxidized Linseed Oil to Bioresin: An Overall Approach of Epoxy/Anhydride Cross-Linking. *ChemSusChem* **2015**, *8*, 1232–1243. [[CrossRef](#)]

14. Grauzeliene, S.; Navaruckiene, A.; Skliutas, E.; Malinauskas, M.; Serra, A.; Ostrauskaite, J. Vegetable Oil-Based Thiol-Ene/Thiol-Epoxy Resins for Laser Direct Writing 3d Micro-/Nano-Lithography. *Polymers* **2021**, *13*, 872. [[CrossRef](#)] [[PubMed](#)]
15. Di Mauro, C.; Tran, T.-N.; Graillot, A.; Mija, A. Enhancing the Recyclability of a Vegetable Oil-Based Epoxy Thermoset through Initiator Influence. *ACS Sustain. Chem. Eng.* **2020**, *8*, 7690–7700. [[CrossRef](#)]
16. Di Mauro, C.; Malburet, S.; Genua, A.; Graillot, A.; Mija, A. Sustainable Series of New Epoxidized Vegetable Oil-Based Thermosets with Chemical Recycling Properties. *Biomacromolecules* **2020**, *21*, 3923–3935. [[CrossRef](#)] [[PubMed](#)]
17. Samper, M.D.; Petrucci, R.; Sánchez-Nacher, L.; Balart, R.; Kenny, J.M. New Environmentally Friendly Composite Laminates with Epoxidized Linseed Oil (ELO) and Slate Fiber Fabrics. *Compos. Part B Eng.* **2015**, *71*, 203–209. [[CrossRef](#)]
18. Dinu, R.; Mija, A. Bio-Based Epoxy Resins and Composites from Epoxidized Linseed Oil Crosslinked with Different Cyclic Anhydrides and Their Combination with Lignin. *Cellul. Chem. Technol.* **2020**, *54*, 925–938. [[CrossRef](#)]
19. Mosiewicki, M.A.; Marcovich, N.E.; Aranguren, M.I. Creep Behavior of Wood Flour Composites Made from Linseed Oil-Based Polyester Thermosets. *J. Appl. Polym. Sci.* **2011**, *121*, 2626–2633. [[CrossRef](#)]
20. Tanase, C.; Talmaciu, A.I.; Băra, C.I.; Boz, I.; Volf, I.; Oroian, S.; Popa, V.I. New Aspects of Biomass Waste Valorization: Spruce Bark Crude Extracts as Plant Growth Regulators. *BioResources* **2018**, *13*, 3994–4007. [[CrossRef](#)]
21. Gößwald, J.; Barbu, M.C.; Petutschnigg, A.; Tudor, E.M. Binderless Thermal Insulation Panels Made of Spruce Bark Fibres. *Polymers* **2021**, *13*, 1799. [[CrossRef](#)]
22. Peng, Y.; Nair, S.S.; Chen, H.; Farnood, R.; Yan, N.; Cao, J. Application of Different Bark Fractions in Polypropylene Composites: UV and Thermal Stability. *Polym. Compos.* **2020**, *41*, 2198–2209. [[CrossRef](#)]
23. Pásztor, Z.; Mohácsiné, I.R.; Gorbacheva, G.; Börcsök, Z. The Utilization of Tree Bark. *BioResources* **2016**, *11*, 7859–7888. [[CrossRef](#)]
24. Zhang, J.; Zheng, Y.; Zhou, H.; Zhang, J.; Zou, J. The Influence of Hydroxylated Carbon Nanotubes on Epoxy Resin Composites. *Adv. Mater. Sci. Eng.* **2012**, *2012*, 518392. [[CrossRef](#)]
25. Liu, J.; An, L. Synthesis and Properties of Graphene/Carbon Nanotube/Epoxy Resin Composites. *Chem. Eng. Trans.* **2018**, *71*, 949–954. [[CrossRef](#)]
26. Yoonessi, M.; Lebroín-Coloín, M.; Scheiman, D.; Meador, M.A. Carbon Nanotube Epoxy Nanocomposites: The Effects of Interfacial Modifications on the Dynamic Mechanical Properties of the Nanocomposites. *ACS Appl. Mater. Interfaces* **2014**, *6*, 16621–16630. [[CrossRef](#)]
27. Nizamuddin, S.; Jadhav, A.; Qureshi, S.S.; Baloch, H.A.; Siddiqui, M.T.H.; Mubarak, N.M.; Griffin, G.; Madapusi, S.; Tanksale, A.; Ahamed, M.I. Synthesis and Characterization of Polylactide/Rice Husk Hydrochar Composite. *Sci. Rep.* **2019**, *9*, 5445. [[CrossRef](#)]
28. Fang, J.; Zhan, L.; Ok, Y.S.; Gao, B. Minireview of Potential Applications of Hydrochar Derived from Hydrothermal Carbonization of Biomass. *J. Ind. Eng. Chem.* **2018**, *57*, 15–21. [[CrossRef](#)]
29. Cai, J.; Li, B.; Chen, C.; Wang, J.; Zhao, M.; Zhang, K. Hydrothermal Carbonization of Tobacco Stalk for Fuel Application. *Bioresour. Technol.* **2016**, *220*, 305–311. [[CrossRef](#)]
30. Khan, T.A.; Saud, A.S.; Jamari, S.S.; Rahim, M.H.A.; Park, J.W.; Kim, H.J. Hydrothermal Carbonization of Lignocellulosic Biomass for Carbon Rich Material Preparation: A Review. *Biomass Bioenergy* **2019**, *130*, 105384. [[CrossRef](#)]
31. Puccini, M.; Stefanelli, E.; Tasca, A.L.; Vitolo, S. Epoxy Composites Based on Low-Cost Carbon Filler Derived from Hydrothermal Carbonization of Waste. *Chem. Eng. Trans.* **2019**, *74*, 1153–1158. [[CrossRef](#)]
32. Nizamuddin, S.; Baloch, H.A.; Griffin, G.J.; Mubarak, N.M.; Bhutto, A.W.; Abro, R.; Mazari, S.A.; Ali, B.S. An Overview of Effect of Process Parameters on Hydrothermal Carbonization of Biomass. *Renew. Sustain. Energy Rev.* **2017**, *73*, 1289–1299. [[CrossRef](#)]
33. Flory, P.J. *Principles of Polymer Chemistry*; Cornell University Press: Ithaca, NY, USA, 1953.
34. Tobolsky, A.V. *Properties and Structure of Polymers*; Wiley: New York, NY, USA, 1960.
35. Matejka, L.; Lovy, J.; Pokorny, S.; Bouchal, K.; Dusek, K. Curing Epoxy Resins With Anhydrides. Model Reactions and Reaction Mechanism. *J. Polym. Sci.* **1983**, *21*, 2873–2885. [[CrossRef](#)]
36. Leukel, J.; Burchard, W.; Krüger, R.P.; Much, H.; Schulz, G. Mechanism of the Anionic Copolymerization of Anhydride-Cured Epoxies—Analyzed by Matrix-Assisted Laser Desorption Ionization Time-of-Flight Mass Spectrometry (MALDI-TOF-MS). *Macromol. Rapid Commun.* **1996**, *17*, 359–366. [[CrossRef](#)]
37. Liu, X.; Xin, W.; Zhang, J. Rosin-Based Acid Anhydrides as Alternatives to Petrochemical Curing Agents. *Green Chem.* **2009**, *11*, 1018. [[CrossRef](#)]
38. Ma, S.; Liu, X.; Fan, L.; Jiang, Y.; Cao, L.; Tang, Z.; Zhu, J. Synthesis and Properties of a Bio-Based Epoxy Resin with High Epoxy Value and Low Viscosity. *ChemSusChem* **2014**, *7*, 555–562. [[CrossRef](#)]
39. Menon, V.; Rao, M. Trends in Bioconversion of Lignocellulose: Biofuels, Platform Chemicals & Biorefinery Concept. *Prog. Energy Combust. Sci.* **2012**, *38*, 522–550. [[CrossRef](#)]
40. Wang, T.; Zhai, Y.; Zhu, Y.; Li, C.; Zeng, G. A Review of the Hydrothermal Carbonization of Biomass Waste for Hydrochar Formation: Process Conditions, Fundamentals, and Physicochemical Properties. *Renew. Sustain. Energy Rev.* **2018**, *90*, 223–247. [[CrossRef](#)]
41. Rojo, E.; Alonso, M.V.; Oliet, M.; Del Saz-Orozco, B.; Rodriguez, F. Effect of Fiber Loading on the Properties of Treated Cellulose Fiber-Reinforced Phenolic Composites. *Compos. Part B Eng.* **2015**, *68*, 185–192. [[CrossRef](#)]
42. Díez, D.; Uruña, A.; Piñero, R.; Barrio, A.; Tamminen, T. Determination of Hemicellulose, Cellulose, and Lignin Content in Different Types of Biomasses by Thermogravimetric Analysis and Pseudocomponent Kinetic Model (TGA-PKM Method). *Processes* **2020**, *8*, 1048. [[CrossRef](#)]

43. Barta-Rajnai, E.; Várhegyi, G.; Wang, L.; Skreiberg, Ø.; Grønli, M.; Czégény, Z. Thermal Decomposition Kinetics of Wood and Bark and Their Torrefied Products. *Energy Fuels* **2017**, *31*, 4024–4034. [[CrossRef](#)]
44. Dorez, G.; Taguet, A.; Ferry, L.; Lopez-Cuesta, J.M. Thermal and Fire Behavior of Natural Fibers/PBS Biocomposites. *Polym. Degrad. Stab.* **2013**, *98*, 87–95. [[CrossRef](#)]
45. De Rosa, I.M.; Santulli, C.; Sarasini, F. Mechanical and Thermal Characterization of Epoxy Composites Reinforced with Random and Quasi-Unidirectional Untreated Phormium Tenax Leaf Fibers. *Mater. Des.* **2010**, *31*, 2397–2405. [[CrossRef](#)]
46. Monteiro, S.N.; Calado, V.; Rodriguez, R.J.S.; Margem, F.M. Thermogravimetric Behavior of Natural Fibers Reinforced Polymer Composites—An Overview. *Mater. Sci. Eng. A* **2012**, *557*, 17–28. [[CrossRef](#)]
47. Pelaez-Samaniego, M.R.; Yadama, V.; Lowell, E.; Espinoza-Herrera, R. A Review of Wood Thermal Pretreatments to Improve Wood Composite Properties. *Wood Sci. Technol.* **2013**, *47*, 1285–1319. [[CrossRef](#)]
48. Ecochard, Y.; Auvergne, R.; Boutevin, B.; Caillol, S. Linseed Oil-Based Thermosets by Aza-Michael Polymerization. *Eur. J. Lipid Sci. Technol.* **2020**, *122*, 1900145. [[CrossRef](#)]
49. Chan, C.M.; Vandi, L.-J.; Pratt, S.; Halley, P.; Richardson, D.; Werker, A.; Laycock, B. Composites of Wood and Biodegradable Thermoplastics: A Review. *Polym. Rev.* **2018**, *58*, 444–494. [[CrossRef](#)]
50. Brostow, W.; Hagg Lobland, H.E.; Narkis, M. Sliding Wear, Viscoelasticity, and Brittleness of Polymers. *J. Mater. Res.* **2006**, *21*, 2422–2428. [[CrossRef](#)]
51. Brostow, W.; Hagg Lobland, H.E. Brittleness of Materials: Implications for Composites and a Relation to Impact Strength. *J. Mater. Sci.* **2010**, *45*, 242–250. [[CrossRef](#)]
52. Brostow, W.; Lobland, H.; Haley, E.; Narkis, M. The Concept of Materials Brittleness and Its Applications. *Polym. Bull.* **2011**, *67*, 1697–1707. [[CrossRef](#)]
53. Moudood, A.; Rahman, A.; Öchsner, A.; Islam, M.; Francucci, G. Flax Fiber and Its Composites: An Overview of Water and Moisture Absorption Impact on Their Performance. *J. Reinf. Plast. Compos.* **2019**, *38*, 323–339. [[CrossRef](#)]
54. Assarar, M.; Scida, D.; El Mahi, A.; Poilâne, C.; Ayad, R. Influence of Water Ageing on Mechanical Properties and Damage Events of Two Reinforced Composite Materials: Flax–Fibres and Glass–Fibres. *Mater. Des.* **2011**, *32*, 788–795. [[CrossRef](#)]
55. Moudood, A.; Rahman, A.; Khanlou, H.M.; Hall, W.; Öchsner, A.; Francucci, G. Environmental Effects on the Durability and the Mechanical Performance of Flax Fiber/Bio-Epoxy Composites. *Compos. Part B Eng.* **2019**, *171*, 284–293. [[CrossRef](#)]
56. Muñoz, E.; García-Manrique, J.A. Water Absorption Behaviour and Its Effect on the Mechanical Properties of Flax Fibre Reinforced Bioepoxy Composites. *Int. J. Polym. Sci.* **2015**, *2015*, 1–10. [[CrossRef](#)]
57. Capiel, G.; Uicich, J.; Fasce, D.; Montemartini, P.E. Diffusion and Hydrolysis Effects during Water Aging on an Epoxy-Anhydride System. *Polym. Degrad. Stab.* **2018**, *153*, 165–171. [[CrossRef](#)]
58. Derome, D.; Rafsanjani, A.; Patera, A.; Guyer, R.; Carmeliet, J. Hygromorphic Behaviour of Cellular Material: Hysteretic Swelling and Shrinkage of Wood Probed by Phase Contrast X-Ray Tomography. *Philos. Mag.* **2012**, *92*, 3680–3698. [[CrossRef](#)]